Biomass Conversion and Biorefinery (2024) 14:5973–5987
https://doi.org/10.1007/s13399-021-01448-3

ORIGINAL ARTICLE

A comprehensive study to understand removal efficiency for Cr^{6+} using magnetic and activated biochar through response surface methodology

Rumi Narzari[1] · Maneesh Kumar Poddar[2] · Neonjyoti Bordoloi[3] · Ajit Kumar Sarmah[4] · Rupam Kataki[1]

Received: 24 November 2020 / Revised: 11 March 2021 / Accepted: 16 March 2021 / Published online: 27 March 2021

Abstract

This study highlights the advantageous effect of magnetic biochar (MLC) over conventional activated biochar (ALC) used for chromium adsorption from the aqueous solution. The synthesis of MLC was done using an invasive noxious weed "*Lantana camara*" with impregnation of iron chloride ($FeCl_3$) on biochar surface at 25 °C. The optimum process parameters such as pH (3.01), adsorbent concentration (1.82 g/L), and adsorbate amount (161.23 mg/L) for the maximum chromium adsorption have been calculated using response surface methodology coupled with central composite design. Successful impregnation of iron on biochar with pre and post adsorption analysis has been confirmed using various characterization techniques viz. vibrating sample magnetometry (VSM), field emission scanning electron microscope (FESEM-EDX), Fourier transform infrared (FTIR), and X-ray diffraction (XRD). Among various adsorption isotherms studied, Langmuir isotherm best fits the pseudo-second-order kinetic model for analysis of actual adsorption behavior of Cr^{6+} ions on ALC and MLC surfaces. Biochar MLC exhibited the maximum chromium adsorption capacity of 102.03 mg/g as compared to low chromium adsorption of 94.69 mg/g using conventional ALC biochar.

Keywords Activated biochar · Adsorption · Chromium · Magnetic biochar · Optimization

1 Introduction

Metal or metalloids with a specific density higher than 5 g/cm^3 can be generally categorized as heavy metals. With the continued increase in heavy metal concentration in the environment due to human activities and at places due to natural occurrences, there exists a serious global threat given the long biological half-life, high toxicity, bio-accumulative nature, and the carcinogenic effects of these compounds [1]. Among all heavy metals, chromium (Cr) is known as one of the major metal pollutants, being present in both surface and groundwater either in single chromium Cr (0) or in heavy metal complex in trivalent (Cr^{3+}) or hexavalent (Cr^{6+}) form. According to the United States Environmental Protection Agency (USEPA), the permissible limit of Cr in potable water is 0.1 mg/L [2], and 0.05 mg/L is limited by the Bureau of Indian Standard [3]. Various industries associated with activities such as alloying, textile dyes and mordants, pigments, ceramic glazes, tanning, electroplating, and many more directly release Cr into the environment through the discharge of wastewater effluent. The hexavalent Cr^{6+} which contains the chromium in +6 oxidation state is considered more vulnerable and highly toxic owing to its greater solubility, high oxidizing potential, and easy mobility across the membranes in living organisms [4, 5]. Exposure of Cr^{6+} to humans or animals in the form of inhalation or drinking water can cause various carcinogenic, mutagenic, and teratogenic effects [6].

Applications of various techniques such as solvent extraction, membrane separation, electrocoagulation, reduction, reverse osmosis, and photo-reduction are employed for removal of Cr from wastewater. However, most of these processes are energy and reagent-intensive, less efficient, and costly [7].

✉ Rupam Kataki
rupamkataki@gmail.com

[1] Department of Energy, Tezpur University, Tezpur, Assam 784028, India

[2] Department of Chemical Engineering, National Institute of Technology, Surathkal 575025, India

[3] Department of Chemistry, Assam Down Town University, Guwahati, Assam 781026, India

[4] Department of Civil & Environmental Engineering, The University of Auckland, Auckland, New Zealand

Therefore, alternative technology and more common method such as adsorption technology is more preferable and widely accepted for Cr^{6+} or metal removal due to its low energy consumption and cost-effectiveness [8, 9]. In this regard, utilization of natural materials such as detox tea waste, acorn shell, eggshell, olive mill waste, peanuts, and brewed tea waste has gained momentum in the recent decade [10–12].

Biochar is a pyrogenic carbon-rich material generated from biomass in the absence of or under limited oxygen conditions. Its porous structure, abundant oxygenated functional groups, aromatic surfaces, high surface-to-volume ratio, and large surface area make biochar an excellent bio-adsorbent suitable for Cr^{6+} adsorption from aqueous solution [13]. The use of biochar as expulsion of metallic contaminants like Pb, Cu, Cd, Zn, Ni, and As from aqueous solutions have been reported earlier by many researchers [4, 14]. The mechanisms during removal of metal ions involve various techniques viz. electrostatic interactions, ionic exchange, precipitation/co-precipitation, and metal complexation with free functional groups involved with physical adsorption [15, 16]. Various studies suggest that the sorption capacity of the pristine biochar is limited and unsatisfactory [5, 17, 18]. Therefore, to further enhance the sorption capacity of biochar, various modified methods have been also developed such as alkali modification, magnetic biochars, and nanoparticle doped biochars [10, 19, 20]. Activation of the pristine biochar potentially has several advantages such as enhancement of its porosity, surface area, electron conductivity, and increased surface functional groups for adsorption process to take place. However, the inability to efficiently remove highly soluble heavy metals from the solution, difficulties associated with adsorbent separation, and longer production duration are some of its drawbacks. In this regard, the use of magnetic biochar could play a significant role as the sorbent could be easily separated by using an external permanent magnetic field and there have been several examples of such available in the literature [16].

Weeds are capable of causing nearly 32% of loss in crop yield in India [21]. *Lantana camara* (LC) is an invasive noxious weed and grows wild in disturbed areas. Loss of biodiversity due to the displacement of native biota, disruption of succession cycle, and allelopathic effect are some of its negative impacts. It is also considered agricultural waste generated during the cultivation of crops and extraction of some medicinal compounds [22–24]. Pyrolytic valorization of this weed can, therefore, be a viable option for its management through its conversion into bio-oil and other co-products such as biochar and syngas [25]. The major structural properties that help in the activation of LC biomass are low inorganic mineral content, high volatile contents, and compactness of the structure; the more the compactness of the material, the lesser the penetration of activation agents [26, 27]. Activation and magnetization of biochar can be achieved via two processes: one-step (pre-pyrolysis) or two-step process (post pyrolysis). Several studies have confirmed that the pre-pyrolysis magnetization of biochar has better sorption ability and stability at varying pH conditions owing to the higher surface area, functional groups, and Fe_3O content in comparison to post pyrolysis [28, 29]. However, in the case of alkali activation, post pyrolysis activation has been found to produce biochar with higher porosity and adsorption capacity as compared to the one-step process [30].

Techniques used for adsorption of Cr^{6+} from wastewater possess various limitations in terms of the requirement of large quantities of adsorbents, unexpected dose amount, and multi-step processing. Optimization of these input variables using response surface methodology (RSM) could be an alternative and the most efficient way to find out the optimum concentration of all input variables for maximum absorbance capacity. Optimization of input variables can be accomplished by employing RSM as a statistical tool [31], though a plethora of work has been conducted to evaluate the removal efficiency of modified biochar over pristine biochar applying various modification techniques such as alkali activation, magnetization, and nano-particle impregnation. However, there is no information available in the literature about the effectiveness of Cr^{6+} removal by magnetic biochar in comparison to activated biochar and the optimization of chromium adsorption on magnetic biochar. The success of any adsorbent can be assessed by its techno-economic feasibility for production at an industrial scale. The production cost of an adsorbent is a vital component in its marketing and application. The lack of information regarding the techno-economic aspect between the lab-scale and pilot-scale production of adsorbents acts as a barrier against real application potential. The major cost that should be considered is production cost, maintenance cost, feedstock cost, transport cost, labor cost, distribution cost, and miscellaneous to ensure long-term industrial practicability [32].

In this work, we have compared the removal efficiency of Cr^{6+} using MLC and ALC biochar as adsorbents. For this, we have optimized and compared the biochars' input process variables such as (i) pH, (ii) adsorbent dose quantity, and (iii) initial metal (Cr) concentration for maximum adsorption efficiency. Also, the interaction effect among various parameters such as pH, dose quantity, and initial concentration of metal ion solution on the adsorption was studied using response surface methodology (RSM). Various adsorption isotherms including Langmuir, Freundlich, and Temkin were also used to study the mechanism of adsorption behavior. We have employed the pre-pyrolysis and post pyrolysis processes for the production of magnetic and activated biochar, respectively. The preliminary adsorption studies showed that modified biochars exhibited better adsorption performance; hence, we did not attempt to optimize the process parameters for pristine biochar (PLC) for comparison. In this article, we have also tried to shed light on the techno-economic aspect of the production of biochar or activated biochar for wastewater

treatment. However, the adsorption FTIR spectra and EDX spectra are been provided in the supplementary material (Fig S1).

2 Materials and methods

2.1 Raw materials

Biomass "*Lantana camara*" (LC) which is an invasive noxious weed was collected from Tezpur University campus, Napaam (26°41/N and 92°50/E) Assam, India. The biomass was washed several times with deionized water (DIW) followed by air-drying for evaporation of the moisture. Subsequently, the biomass was firstly chopped into small pieces (0.5–1.5 cm) and then reduced into size ~ 0.2 mm using a grinder (Willy mill, SECOR Scientific Eng. Co.). The ground biomass samples were oven-dried at 105 °C for 24 h and stored in a desiccator for further synthesis of activated and magnetic biochar.

2.2 Synthesis of Activated Biochar

The biochar was prepared in a fixed bed tubular quartz reactor (300 mm × 24.7 mm × 2.3 mm) following the protocol developed by Bordoloi et al. [33]. The detailed information on the biochar preparation is given in the supplementary material. Briefly, 40 ml of 4 M sodium hydroxide (NaOH) aqueous solution was added to 3 g of biochar, mixed thoroughly at room temperature for 2 h, and shaken at a regular interval of 15 min. The mixture was filtered using a vacuum filter and dried overnight in an oven at 105 °C. The dried sample was heated in the quartz-tube reactor at 800 °C with a heating rate of 3 °C/min under inert atmospheric conditions (2 L/min N_2 flow) for 2 h. The activated sample was cooled, washed with DIW followed by 0.1 M HCl solution, and repeated several times with DIW until the pH of the filtrate was neutral. The samples were dried in an oven and stored in a desiccator and hereafter referred to as ALC [34].

2.3 Synthesis of Magnetic Biochar

The raw biomass (10 g) was soaked for 2 h in a ferric chloride solution (40 g of $FeCl_3 \cdot 6H_2O$ in 60 ml of DI water) at room temperature. The soaked biomass composites with irons were vacuum-dried at 80 °C for 6 h followed by pyrolysis at 500 °C for 1 h [19]. The composites of pyrolyzed biochar were further crushed, sieved, and washed with DIW to remove any impurities present. Finally, the composites of magnetic biochar were dried at 80 °C and sealed in a desiccator for further analysis.

2.4 Multivariate Experimental Design

RSM was employed to optimize the three independent variables viz, (1) solution pH, (2) adsorbent dosage, and (3) initial metal (Cr) concentration in the solution for maximum adsorbate removal efficiency of ALC and MLC (Table 1). The actual and coded values ($-\alpha$, -1, 0, $+1$, $+\alpha$) of these independent variables using central composite design (CCD) in Design-Expert software (Version 10.0.6, Stat-Ease Inc., MN, USA) are reported in Table 2.

The process parameters of the study were selected based on similar studies reported in the literature [4, 35]. Using the CCD, the total estimated experimental design was constituted of 20 individual runs. The experiment was repeated three times with the minimum standard deviation to ensure statistical significance of the results. The response variables of both ALC and MLC were fitted with the use of generalized second-order polynomial equation, including the interaction effect of variables as shown below:

$$Y(\%) = \beta b_o + \sum_{i=1}^{n} \beta_i X_i + \sum_{i=1}^{n} \beta_{ii} X^2{}_i + \sum_{i=1}^{n} \sum_{j>1}^{n} \beta_{ij} X_i X_j + e \quad (1)$$

where Y = predicted removal efficiency, β_0 = constant coefficients, β_i = linear coefficients, β_{ii} = quadratic coefficients, β_{ij} = interaction coefficients, n= total number of experiments, and X_i and X_j are coded independent factor.

2.5 Characterization

The proximate and ultimate analysis of the raw biomass and its respective biochars were performed following the ASTM D3172-07a method. Parameters such as pH and electrical conductivity were measured using a pH meter (EUTECH Instruments pH 700) and a conductivity meter (Digital TDS/Conductivity Meter MK509). The carbon sequestration potential of biochar was determined by considering the R_{50} index as reported elsewhere [33]. Zero-point charge (ZPC) of adsorbent was determined by salt addition method [14]. The surface area of the biochar samples was measured from N_2 adsorption data by using a gas sorption analyzer (NOVA-1000E; Quanta

Table 1 Experimental factors and level used in the CCD

Variables	Symbols	Levels				
		$-\alpha$	-1	0	$+1$	$+\alpha$
pH	A	0.954	3	6	9	11.045
Dose (g/L)	B	0.022	0.5	1.2	1.9	2.377
Initial conc.(mg/L)	C	0.570	50	122.5	195	244.43

Table 2 Experimental design matrix using central composite design for three independent variables

Sl. no.	A pH	B Dose (g/L)	C Initial conc. (mg/L)	MLC (%) Experimental	MLC (%) Fitted by model	ALC (%) Experimental	ALC (%) Fitted by model
1	9 (+1)	0.5 (−1)	195 (−1)	57.65 ± 0.10	58.543	47.20 ± 0.08	46.974
2	6 (0)	1.2 (0)	122.5 (0)	83.74 ± 0.07	84.687	68.58 ± 0.11	74.605
3	11.04 (+α)	1.2 (0)	122.5 (0)	47.85 ± 0.14	46.892	40.43 ± 0.04	39.174
4	6 (0)	1.2 (0)	224.4 (+α)	81.50 ± 0.06	82.227	74.32 ± 0.03	74.055
5	9 (+1)	1.9 (+1)	50 (−1)	55.92 ± 0.05	58.589	55.54 ± 0.08	55.597
6	6 (0)	1.2 (0)	0.57 (−α)	69.65 ± 0.09	72.454	56.76 ± 0.02	61.336
7	6 (0)	1.2 (0)	122.5 (0)	84.73 ±0.21	84.687	76.43 ± 0.04	74.605
8	6 (0)	1.2 (0)	122.5 (0)	88.73 ± 0.08	84.687	72.64 ± 0.12	74.605
9	6 (0)	1.2 (0)	122.5 (0)	80.62 ± 0.13	84.687	74.77 ± 0.14	74.605
10	9 (+1)	0.5 (−1)	50 (−1)	60.32 ± 0.21	56.379	44.87 ± 0.11	42.420
11	6 (0)	1.2 (0)	122.5 (0)	85.91 ±0.06	84.687	76.86 ± 0.05	74.605
12	3 (−1)	0.5 (−1)	195 (+1)	84.07 ± 0.09	80.204	79.98 ± 0.04	77.831
13	3 (−1)	1.9 (+1)	50 (−1)	93.42 ± 0.08	91.330	81.90 ± 0.04	80.035
14	6 (0)	0.02 (−α)	122.5 (0)	60.40 ± 0.12	65.316	52.20 ± 0.13	57.113
15	3 (−1)	1.9 (+1)	195 (+1)	95.76 ± 0.08	98.554	88.64 ± 0.07	88.999
16	9 (+1)	1.9 (+1)	195 (+1)	61.87 ± 0.04	62.947	56.87 ±0.06	59.911
17	6 (0)	2.37 (+α)	122.5 (0)	85.87 ± 0.05	82.647	79.54 ± 0.04	77.585
18	3 (−1)	0.5 (−1)	50 (−1)	77.40 ± 0.07	75.126	73.76 ± 0.12	68.627
19	6 (0)	1.2 (0)	122.5 (0)	84.98 ± 0.02	84.687	78.86 ± 0.24	74.605
20	0.954 (−α)	1.2 (0)	122.5 (0)	89.98 ± 0.04	92.635	81.45 ± 0.09	85.667

Numbers in the bracket represent coded values of the variables, while numbers outside the bracket represent the actual value of the parameter (for details, refer to Table 1)

chrome Corp.). Before conducting the measurements, the samples were degassed for 6 h under vacuum at 473 K temperature. Fourier transform infrared (FT-IR) spectroscopy (Nicolet IR spectrometer) was used to determine the surface functionality of biochars. The infrared spectra were collected at room temperature (26 ± 2 °C) in the spectral range of 400–4000 cm^{-1}. The surface physical morphology was examined using a field emission scanning electron microscope (FE-SEM; Sigma, Zeiss). X-ray diffraction (XRD) measurements were conducted on the powders using a Bruker Axs D8 Focus instrument. Vibrating sample magnetometry (VSM; Lakeshore, Model: 7410 series) was performed on both MLC and ALC biochar to determine magnetic property.

2.6 Batch adsorption experiments

The adsorption experiments were carried out using a batch procedure with 50 ml of the metal ions solutions in a 250-ml Erlenmeyer flask at varying pH, dose, and initial concentration as shown in Table 1. The solution was agitated at 150 rpm at room temperature. The stock solution of 1000 mg/L Cr^{6+} was prepared by dissolving analytical grade $K_2Cr_2O_7$ in DIW. All working solutions were freshly prepared before use by diluting the stock solution with DIW, and the pH was adjusted with dropwise addition of HCl or NaOH solutions. The concentration of Cr^{6+} was analyzed with UV–VIS spectrophotometer at a wavelength of 540 nm by using 1,5 diphenylcarbohyhydrazide (UV-2450, SHIMADZU). The amount of Cr^{6+} adsorbed on the samples was estimated by measuring the difference in the initial (C_o) and the equilibrium solute concentration (C_e). The adsorption capacity (q) and the amount of the Cr^{6+} adsorbed from the solution using the following equations [36]:

$$\text{Removal}\% = \frac{(C_o\text{-}C_e)100}{C_o} \tag{2}$$

$$q_e = \frac{(C_o\text{-}C_e)V}{m} \tag{3}$$

where C_o= initial concentration of Cr^{6+} (mg/L), C = concentration of Cr^{6+} at any time (mg/L), C_e= equilibrium concentration of Cr^{6+} (mg/L), q_e = adsorption capacity (mg/g), V = volume of Cr^{6+} solution (L), and m= weight of the adsorbent (g).

The kinetic experiments were also carried out as similar to equilibrium isotherm. The amount adsorbed at time t, q_t (mg/g) was calculated using Eq. (4):

$$q_t = \frac{(C_o\text{-}C_t)V}{m} \quad (4)$$

where C_o and C_t are the liquid-phase concentration at the initial and any time t, respectively.

2.7 Reusability experiment

To study the reusability of the adsorbent, batch desorption experiments were performed. In this, the treated adsorbent was added in 50 ml of 0.5 M NaOH solution followed by mixing at 30 °C for 240 min. The dispersed solution was filtered and the filtrate's metal ion concentration was evaluated using AAS. The adsorbent was washed and again 4 such cycles of adsorption-desorption were repeated. Desorption efficiency is given as:

$$W_{desorption}, \% = \frac{Q_e}{Q_{de}}100 \quad (5)$$

where $W_{desorption}$= desorption efficiency, Q_e = adsorption capacity, and Q_{de}= desorption capacity.

3 Results and discussion

3.1 Optimization of adsorbate removal efficiency

The response of actual and predicted chromium removal efficiency using MLC and ALC using three independent variables are shown in Table 2.

Based on the highest order polynomial, a second-order quadratic regression model was suggested by the software for Cr^{6+} removal efficiency of both MLC and ALC responses. The fitted Eqs. (6) and (7) are as follows:

$$\begin{aligned} Y\ (\mathrm{MLC}\%) = {} & 45.67 + 4.89A + 34.56B + 0.17C \\ & -0.58A^2 - 7.72B^2 - 5.56C^2 \\ & -1.66AB - 0.003\ AC + 0.01BC \end{aligned} \quad (6)$$

$$\begin{aligned} Y\ (\mathrm{ALC}\%) = {} & 51.09 + 1.53A + 20.14B \\ & + 0.17C - 0.47A^2 - 5.23B^2 - 5.10C^2 \\ & + 0.21AB - 5.34\ AC - 1.18\ BC \end{aligned} \quad (7)$$

An examination of the data from Table 2 reveals that the responses of removal efficiency obtained via quadratic model fit matched closely the measured datasets. The fitness of the model can also be confirmed from the parity chart with the majority of values close to the 45° line from the origin (supplementary Fig. S2). It was also observed that the coefficient of variance (C.V.)% for MLC (4.92) and ALC (6.36) was <10% implying that the models are reproducible [37]. The determinant coefficients for MLC (R^2= 0.962, $R^2_{(adj)}$= 0.948, $R^2_{(pred)}$= 0.936) and ALC (R^2= 0.951, $R^2_{(adj)}$= 0.929, and $R^2_{(pred)}$= 0.763) from Table 3 and Table 4 signify that the model fits well to the experimental data. It also suggests that above 90% of the removal efficiency of both the adsorbent is influenced by the process parameters. The positive model terms represent an increase in response to the increase in the optimization parameter, while the negative coefficients are inversely proportional to the response. The parameter obtained from the analysis of variance (ANOVA) table indicates the significance for MLC and ALC. The high F-value and p value >0.05 for "Lack-of-fit" indicate that the regression model is valid for chromium removal [38].

3.2 Influence of the single and interaction variables

The response surface 3-D plots for MLC with the interaction of all three variables are depicted in Fig. 1a–c. Similarly, the response surface 3-D plots for ALC with the interaction of all three variables are depicted in Supplementary Fig. S3A-C.

3.2.1 Effect of pH

During adsorption of metal ions onto biochar, pH plays an important role that affects the dissociation of functional groups, surface charge, and degree of ionization of contaminants on the active adsorbent sites. The negative coefficients of pH values −13.6 and −13.82 for MLC and ALC, respectively, obtained from ANOVA shown in Tables 3A and 4A, illustrate the reduction in removal efficiency with an increase in solution pH. This implies that the metal (Cr^{6+}) removal efficiency (%) using both ALC and MLC has an inverse relationship to the solution pH. The highest Cr^{6+} removal was observed at pH ~3 for both MLC and ALC. We observed that with the increase in pH, the Removal% increased from 89% at pH 1 to 95% at pH 3 for MLC and then exhibited a decline with a further increase in pH value. This behavior may be attributed to the fact that under acidic conditions, the dominant species of Cr in aqueous solution is $HCrO^-_4$ and $Cr_2O_7^{2-}$ while the adsorbent is positively charged below pH 4, causing electrostatic attractions among the adsorbate and adsorbent [39]. The low adsorption free energy for $HCrO^-_4$ compared to CrO_4^{2-} facilitates its adsorption even at the same concentration [40]. Cr^{6+} reduction into Cr^{3+} is caused by electrons present in carbon atomic ring and high redox potential value [41]. The presence of persistent free radical (PFR) and surface functional groups (C–O, C–O–C, and O–C–O bonds) in biochar is responsible for electron acceptance, donation, and shuttle [42]. These functional groups consist of π-electron, whereas PFRs act as free electrons due to the presence of unpaired electrons in the core atoms [43, 44]. Therefore, it can be inferred that PFRs and aromatic π-conjugated systems

Table 3 Analysis of variance (ANOVA), regression coefficient estimate, and test of significance for Cr^{6+} removal

(A) Model coefficients, *t*- and *p*-values for second-order regression model (MLC)				
Model term		Coefficient	*t*-value	*p*-value prob>*F*
Constant		86.69	54.99	0.000
Linear coefficients				
A-pH		−13.60	−13.33	0.000
B-dose		6.09	5.20	0.005
C-initial conc.		2.36	2.31	0.043
Square coefficients				
pH×pH (A^2)		−5.28	−5.33	0.000
Dose×dose (B^2)		−3.78	−3.82	0.003
Initial conc.× initial conc. (C^2)		−2.92	−2.95	0.014
Interaction coefficients				
pH and dose (A×B)		−3.49	−2.62	0.025
pH and initial conc. (A×C)		−0.72	−0.54	0.602
Dose and initial conc. (B×C)		0.54	0.41	0.695
(B) ANOVA for the quadratic model				
Source	DF	SS	MS	*F*-value	*p*-value prob>*F*
Regression	9	3989.45	409.94	28.88	0.000
Linear	3	2964.82	988.27	18.25	0.000
Square	3	103.64	34.55	0.59	0.633
Interaction	3	620.99	207.00	14.58	0.000
Residual (error)	10	141.96	14.20		
Lack-of-fit	5	108.94	21.79	3.30	0.108
Pure error	5	33.02	6.60		
Total	19	3831.41			

DF degree of freedom, *SS* sum of squares, *MS* mean square

*Significant *p* values, $p \leq 0.05$; $R^2 = 0.952$; $R^2_{(adj)} = 0.948$, $R^2_{(pred)} = 0.936$

on the biochars facilitate reduction of Cr^{6+} into Cr^{3+} via transfer of electrons [45, 46] and has been shown through the following equations:

$$R\text{–}OH_2^+ + HCrO_4^- \leftrightarrow R\text{–}OH_2Cr_4^- + H^+ \quad (8)$$

$$HCrO_4^- + 7H^+ + 3e^- \leftrightarrow Cr^{3+} + 4H_2O \quad (9)$$

$$CrO_4^{2-} + 8H^+ + 3e^- \leftrightarrow Cr^{3+} + 4H_2O \quad (10)$$

Here, the electrons are provided by the biochar. Apart from this, impregnation of iron on biochar results in the formation of PFRs that reduces Fe^{3+} into Fe^{2+} which in turn facilitate the reduction of Cr^{6+} [46]. Biochar also acts as an electron shuttle via two mechanisms viz. Geo-battery and geo-conductor results from the redox cycle of functional groups and the direct electron transfer of graphic regions, respectively [47]. Cr^{6+} in the acidic pH is mostly in the form of $HCrO_4^-$, CrO_7^{2-}, and H_2CrO_4 and that can be reduced into $Cr^{3+}$from the electron (e^-) received from the negatively charged biochar surface. The adsorption of Cr^{6+} decreases at high pH due to electrostatic repulsion between Cr^{6+} and negatively charged biochar surface and hence acidic adsorption at acidic pH is more preferable [48] as shown in Eqs. (9) and (10). Reduced Cr^{3+} forms more stable chelate bonds compared to Cr^{6+} with the adsorbent [49]. The decrease in the Cr^{6+} removal% from 95% at pH 3 to 47.8% at pH 11 might be caused by the presence of various other groups of FeOH on the surface of MLC resulting in electrostatic repulsion between $HCrO_4^-$ and positively charged MLC. In the case of ALC, the increase in $^-$OH groups hinders the diffusion of dichromate ions, thereby decreasing removal efficiency. Another explanation is the complexation between Cr^{6+} and carboxylate surface groups which might be responsible for the enhanced adsorption observed in the MLC [40]. The interaction effect of pH with dosage amount and initial adsorbate concentration initially shows that there is an enhancement in Cr^{6+} adsorption efficiency with an increase in pH and thereafter it decreases after attaining the maximum value. Another possible reason for an increase in adsorption could be due to the simultaneous reduction and adsorption of hexavalent chromium (Cr^{6+}) in the presence of positively charged ALC and MLC biochars. A study of reduction and adsorption of hexavalent chromium (Cr^{6+}) in presence of thiol functionalized hybrid material is recently reported by Ifthikar et al. [44, 46]. In their study, the authors have reported the simultaneous reduction of $Cr_2O_7^{2-}$ into Cr^{3+} along with

Table 4 Analysis of variance (ANOVA), regression coefficient estimate, and test of significance for Cr^{6+} removal

(A) Model coefficients, *t*- and *p*-values for second-order regression model (ALC)				
Model term		Coefficient	*t*-value	*p*-value prob>*F*
Constant		74.61	42.15	0.000
Linear coefficients				
A-pH		−13.82	11.81	0.000
b-dose		5.15	5.04	0.000
C-initial conc.		3.38	2.88	0.016
Square coefficients				
pH×pH (A^2)		−4.31	−3.78	0.003
Dose×dose (B^2)		−2.57	−2.25	0.048
Initial conc.× initial conc. (C^2)		−2.68	−2.35	0.040
Interaction coefficients				
pH and dose (A×B)		0.44	0.28	0.778
pH and initial conc. (A×C)		−1.16	−0.75	0.465
Dose and initial conc. (B×C)		−0.06	−0.03	0.969
(B) ANOVA for the quadratic model				
Source	DF	SS	MS	*F*-value	*p*-value prob>*F*
Regression	9	3680.38	408.93	21.81	0.000
Linear	3	3271.59	1090.53	29.26	0.000
Square	3	12.41	4.14	0.09	0.963
Interaction	3	396.39	132.13	7.05	0.007
Residual (error)	10	187.48	18.75		
Lack-of-fit	5	120.81	24.16	1.81	0.265
Pure error	5	66.67	13.33		
Total	19	3867.86			

DF degree of freedom, *SS* sum of squares, *MS* mean square

*Significant *p* values, $p \leq 0.05$; $R^2 = 0.962$; $R^2_{(adj)} = 0.929$, and $R^2_{(pred)} = 0.763$

adsorption of Cr species into a functionalized hybrid in acidic pH 3. From a detailed kinetic study using various kinetic models, it has been concluded that the reduction of $Cr_2O_7^{2-}$ into Cr^{3+} is faster as compared to the adsorption of $Cr_2O_7^{2-}$ into Cr^{3+}.

3.2.2 Effect of adsorbent dosage

The positive coefficient of dosage amount obtained from ANOVA as summarized in Table 3 and Table 4A illustrated that an increase in the dosage concentration increased the metal removal efficiency using both ALC and MLC biochar due to enhancement in surface area and adsorption sites of the biochar. However, as compared to the ALC biochar, MLC is presumed to be more effective because of high coefficient dosage value of 6.09 overdosage value of 5.15 using ALC (Table 3 and Table 4). The increase in the removal efficiency with the increase in the adsorbent indicates the increase in binding/exchangeable sites [50]. However, a reduction in removal efficiency after the optimum point is due to the overlapping of active sites caused by crowding of adsorbents [51]. Additionally, the high H/C, O/C ratio, and presence of oxygen-containing acidic functional groups (carboxyl and/or hydroxyl) in MLC enable metal chelation. Hence, it can be inferred that the number of exchange sites in the MLC is greater than the ALC.

3.2.3 Effect of initial concentration

The results of the effect of the initial concentration of Cr^{6+} on metal removal efficiency using both biochars ALC (3.38) and MLC (2.36) showed a similar behavior as the adsorbent dose effect. With the increase in the initial concentration of Cr^{6+}, the removal percentage of metal ions using both MLC and ALC decreased. A plausible explanation for this could be due to the unavailability of adequate adsorption sites which is solely responsible for the binding of the metal ions. The trend of percentage reduction in metal removal by both biochars was observed to be similar. This finding is observed in Figs. 1B-C and S3B-C (supplementary), for MLC and ALC, respectively.

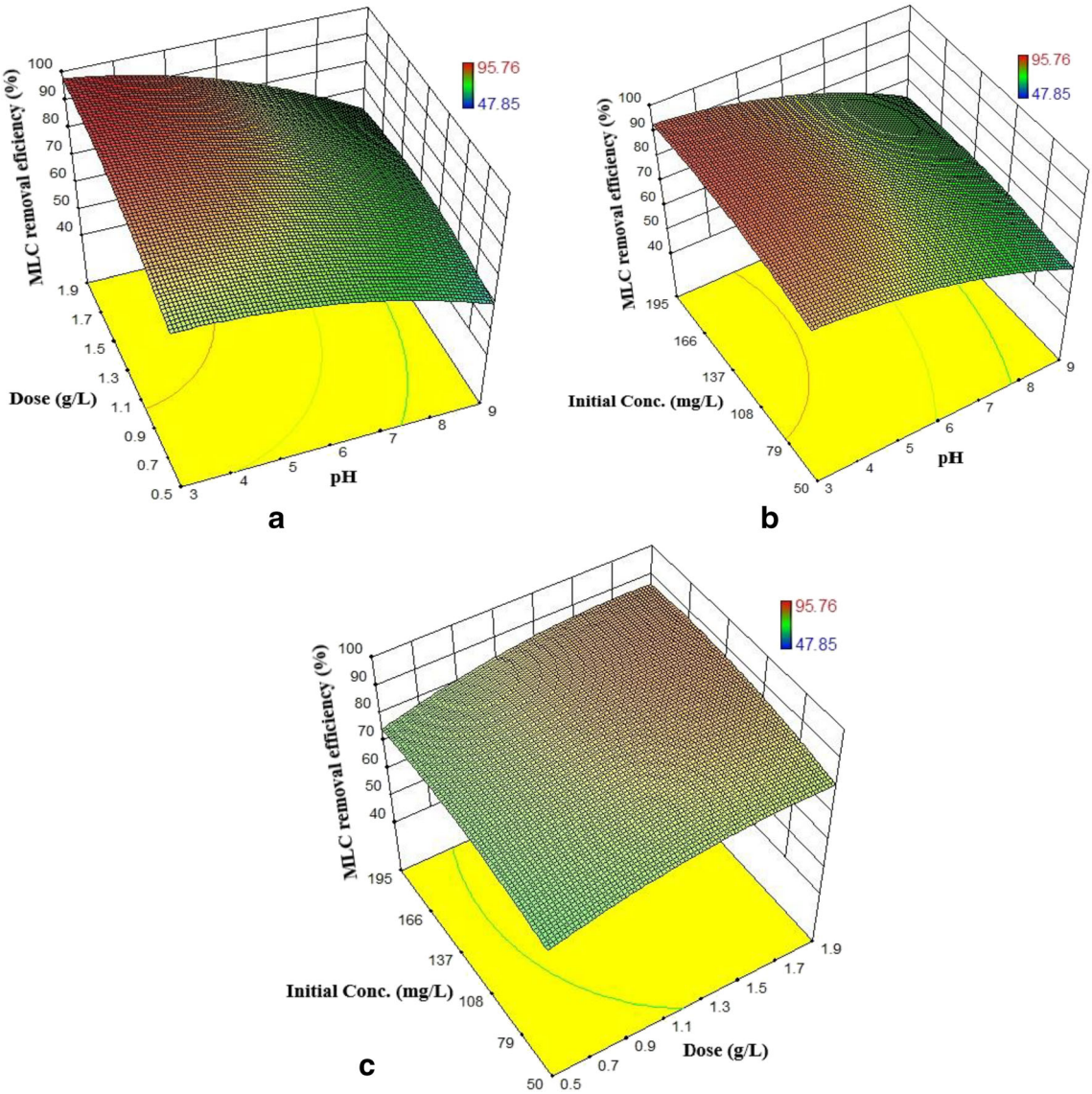

Fig. 1 Response surface plots for MLC as a function of any two experimental parameters: **a** pH and adsorbent dose, **b** pH and initial concentration of adsorbate, **c** adsorbent dosage and initial concentration of adsorbate

3.3 Validation of experiments with the optimized parameters

The highest experimental removal efficiency for both MLC and ALC under optimized conditions was 98.7% and 96.32%, while predicted values were 88.7% and 86.57% respectively. Although we did not perform dedicated parameter optimization for PLC but under the optimum condition obtained for MLC and ALC, PLC showed removal efficiency 69.2%. These results suggest that the statistical analysis of the operational condition predicted by the CCD is in good agreement with the experimental data. The optimum adsorption conditions obtained for both MLC and ALC for maximum removal were as follows: pH = 3.01, an initial concentration of 161.23 mg/L, and a dose of 1.82 g/L (Supplementary Fig. S4).

3.4 Characterization of adsorbents

The results of BET surface area (Table 5) shows a very high surface area in ALC (607.53 m^2/g) as compared to MLC (323.02 m^2/g) and PLC (151.06 m^2/g). The high surface area in ALC could be attributed to the reopening of all blocked pores during the high-temperature activation process. The high-velocity gases evolved during the activation process could enter into the jammed pores and most likely cleaned them thoroughly due to thermal diffusion and ultimately increasing biochar porosity [50]. Even though both the biochars (MLC and ALC) were produced at the same temperature, however, the bulk carbon content (Table 5) in MLC was found to be relatively lower than ALC, i.e., 58.72% and 65.86%, respectively. This could be attributed to the dilution

Table 5 Physicochemical properties biochars before and after modification

Properties	Raw biomass	PLC	ALC	MLC
Proximate analysis (%)				
Moisture	3.41 ±2.1	1.49 ±0.3	1.48 ±0.6	1.49 ±1.5
Volatile matter	75.33 ±0.4	42.41 ±0.7	15.8 ±1.8	36.61 ±1.8
Ash	4.31 ±1.7	9.40 ±0.3	11.5 ±0.9	20.70 ±2.7
Fixed carbon	16.95 ±2.4	46.70 ±0.3	71.22 ±1.1	41.50 ±3.9
Ultimate analysis (%)				
C	45.59 ±4.2	60.81 ±1.0	65.86 ±0.9	58.72±2.7
H	5.84 ±1.0	1.87 ±3.7	2.75 ±1.3	2.88±1.8
N	0.72 ±3.7	2.57 ±2.3	5.79 ±4.1	1.97±5.8
O	47.84 ±1.5	34.75 ±1.8	25.60±3.6	36.43 ±2.4
H/C	1.59	0.37	0.50	0.59
O/C	0.79	0.43	0.29	0.47
pH	–	7.65 ±0.04	10.25±0.2	6.82 ±0.1
EC (dS/m)	–	0.85 ±0.71	1.11 ±1	0.79 ±0.5
BET Surface area (m^2/g)	–	151.06	607.53	323.02
CEC (mmol/kg)	–	84.40±3	655 ± 10	366 ± 2
PZC	–	3.75 ±0.1	4.1 ±0.02	3.17 ±0.10
R_{50}	0.24	0.54	0.61	0.57
CSP (%)	17.00	25.00	42.10	40.10

PZC pH of zero point charge, *CEC* cation exchange capacity, *CV* calorific value, R_{50} recalcitrance index, *CSP* carbon sequestration potential, *EC* electrical conductivity

effect caused by impregnation of Fe on MLC surface which was verified by the presence of high ash content viz. 20.7 wt% for MLC while it is 11.5 wt% for ALC [20]. MLC which exhibits a high O/C ratio of 0.47 as compared to the ALC (O/C of 0.29) indicates its high degree of polarity, owing to the occurrence of a huge number of oxygen-containing functional groups [16]. However, the decline in O/C ratio for ALC means that with the increase in aromaticity, there is an increase in hydrophobicity resulting in cross-linking of adsorbent surface and activation agent. The increase in N contents could also lead to the formation of more functional groups containing nitrogen which enhances adsorption of negatively charged ions [29].

The FTIR spectra of PLC, ALC, and MLC biochar before and after adsorption are shown in Fig. 2. Broad peaks present in both MLC and ALC in the range of 400–580 cm^{-1} correspond to the presence of alkyl halides. There is a disappearance of a strong and sharp band at 469 cm^{-1} and a weak band at 2345 cm^{-1} in the pristine biochar after its modification which is assigned to Si–O of silicates and CO_2, respectively [52]. The adsorption bands at 1419–1420 cm^{-1} present in PLC and ALC corresponds to symmetric stretching of phenolic compounds. The increases in the projection in the fingerprint region (400–1400 cm^{-1}) in MLC are ascribed for iron oxide, and it signified the successful impregnation of iron oxide [53]. However, these bands are absent in ALC. The appearance of a weak band at 1585 cm^{-1} in MLC and its absence in ALC represents the conjugated C=C stretching vibration. The presence of 585 cm^{-1} represents H_2N–C=O in ALC and MLC provides protons for reduction of Cr^{6+}. The broadband in the range of 3400–3700 cm^{-1} indicates the existence of hydroxyl group which weekend and nearly disappeared in the MLC biochar after sorption which confirms its involvement in the sorption of Cr^{6+} [52]. The peak, which is assigned to aromatic C=C stretching appeared at 1400–1600 cm^{-1} in MLC both before and after adsorption while in ALC, was absent before adsorption and reappeared after Cr^{6+} loading. The functional groups assigned for –CH, –OH, and –CO which is solely responsible for Cr absorption were also verified by the presence of spectrum peak at 3000, 3400, and 1050 cm^{-1}on the biochars [6, 10].

The X-ray diffractograms of both MLC and ALC biochars are depicted in Fig. 3a. The XRD patterns for biochars show an absence of sharp crystalline cellulosic peak [2θ = 22.7°] confirms decomposition of cellulose resulting in amorphous structure in the biochar [54]. The MLC biochar shows a crystalline structure with the presence of various sharp peaks at 2θ values of 35.5, 43.2, 57.3, and 62.9° which verify the entities of maghemite [55]. These peaks were present in XRD of both pre and post adsorbed biochars (Fig. 3a). However, no changes in the crystallinity of biochar were observed before and after the adsorption process, which confirmed the strong impingement of iron oxide on its surface. On the other hand, ALC biochar showed a broad peak at 2θ values of 24.8° and

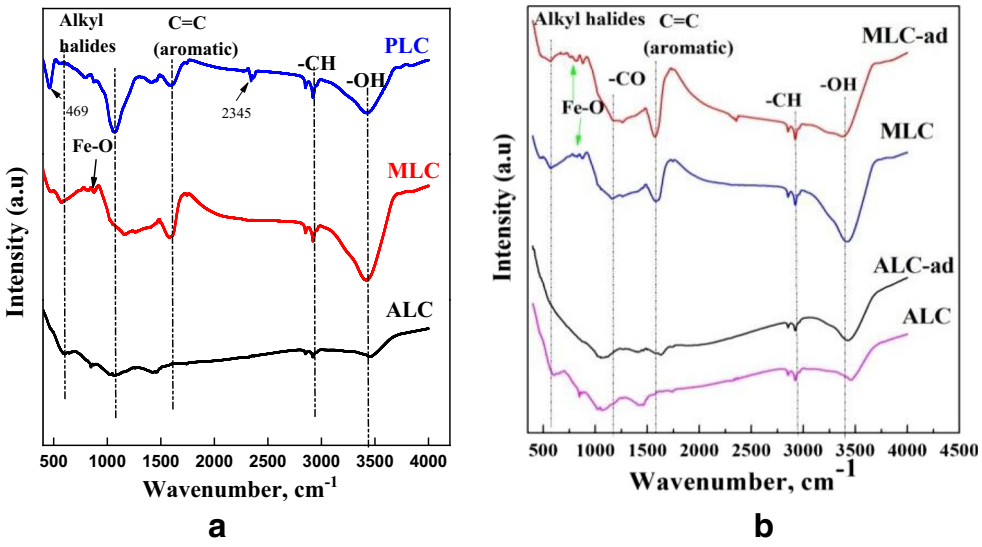

Fig. 2 FTIR spectra. **a** Before adsorption and **b** after adsorption

42.4° caused due to lattice contraction caused by NaOH treatment [24].

To confirm the successful impregnation of magnetic particles on biochar using iron chloride, the magnetization experiments of both MLC and ALC biochars were carried out using VSM at room temperature and the results of M-H curves are depicted in Fig. 3b. As compared to almost zero magnetization saturation (M_S) obtained using ALC biochar, MLC biochar shows a high M_s of 4.5 emu/g which attributes its strong ferromagnetic behavior. The high M_s value of MLC confirms

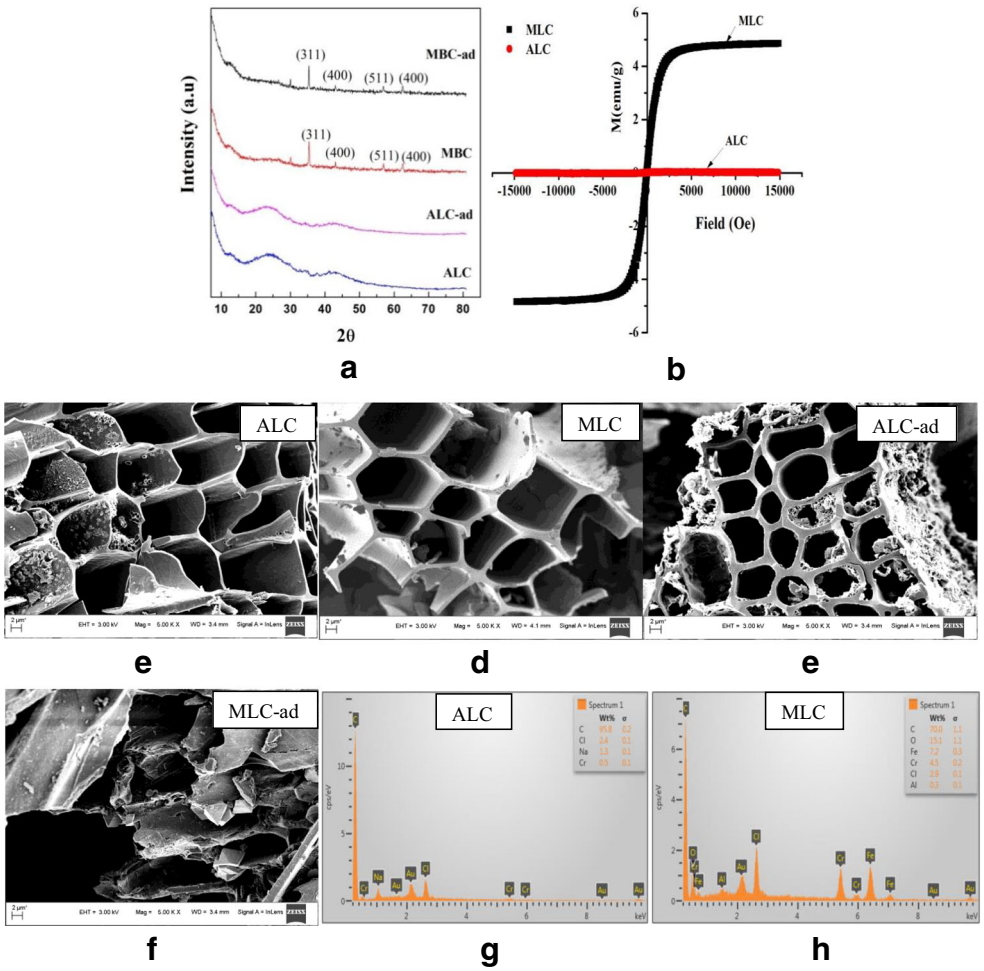

Fig. 3 Characterization of modified biochar with and without Cr^{6+} loading. **a** X-ray diffractograms; **b** magnetization curves; **c**, **d** FESEM images before adsorption; **e**, **f** FESEM images after adsorption; **g**, **h** EDX images after adsorption

the impregnation of magnetic particles on the MLC biochar during synthesis with iron chloride.

FESEM images were used to observe the morphological structure of the adsorbent before and after the adsorption. As can be observed from Fig. 4c, the pores present in ALC which are adsorbent's surfaces before adsorption are unoccupied; however, the micrograph shown in Fig. 4e showed the occupancy of pores with Cr^{6+} after the adsorption [15]. The EDX spectrum of both the biochars after adsorption (Fig. 4g, h) verifies the loading of Cr^{6+} in both biochars (ALC and MLC). The presence of Fe peaks in MLC also confirms the successful impingement of magnetic particles on biochar. The pH and point of zero charge (PZC) decrease in the MLC (3.17) biochar after magnetic modification due to the presence of magnetite and its oxidation. Further, the MLC biochar also exhibited an increased cation exchange capacity (CEC) due to a high CEC value of iron oxide [13]. MLC biochar can be easily separated from the aqueous solution by using an external paramagnetic field, while ALC showed no response. Hence, a magnetic separation technique can be applied to separate magnetic biochar after adsorption [19]; however, the potential application is far from being demonstrated at pilot scale.

3.5 Adsorption isotherms

An adsorption isotherm describes the interaction between adsorbate molecules and the adsorbent at equilibrium conditions at a constant temperature. It explains the mass transfer phenomenon of adsorbate from one phase when equilibrium is established in between both phases at a constant temperature. In our study, three equilibrium isotherm models viz. Langmuir, Freundlich, and Temkin isotherm have been used to explain the distribution of the adsorbate (Cr^{6+}) present in the aqueous phase to the surface of solid adsorbents (biochars), at equilibrium. The models are based on the assumption related to homogeneity/heterogeneity of adsorbent surface, type of surface coverage, and interaction among the adsorbate. The model depends on the way the adsorption heat decreases across the surface coverage viz. Langmuir with no decrease at all; Freundlich assumes a logarithmic decrease, while Temkin assumes a linear decrease [36]. In this study, the suitable isotherm models were evaluated by fitting the experimental data with the different isotherms of Langmuir, Freundlich, and Temkin adsorption isotherm (supplementary Fig. S5).

The non-linear mathematical equation for Langmuir isotherm is as follows [50]:

$$q_e = q_m b C_e/(1 + bC_e) \quad (11)$$

where q_m =maximum adsorption capacity (mg/g); b= Langmuir constants (L/mg); C_e= equilibrium concentration of adsorbate (mg/L); and q_e= amount of metal adsorbed per gram of the adsorbent at equilibrium (mg/g).

The expression for Freundlich isotherm can be given as:

$$q_e = K_f C_e^{1/n} \quad (12)$$

where K_f signifies Freundlich isotherm constants associated with adsorption capacity (mg/g) and $1/n$ denotes the sorption intensity [33].

The Temkin isotherm model can be represented as [56]:

$$q_e = (RT/b)[\log(K_t C_e)] \quad (13)$$

where b=Temkin isotherm constant, R= gas constant (8.314 J/mol/K), and T = temperature (298 K).

From Table 6, it is evident that both MLC and ALC can be well explained to Langmuir adsorption isotherm. The "fitness of good" for MLC and ALC are 0.991 and 0.994, respectively, which is higher than the other two adsorption isotherm. According to the Langmuir model, sorption of metal ion occurs on a homogenous surface by monolayer adsorption with no interaction among adsorbate with uniform sorption activation energy. The limiting reaction step is the surface reaction as in the heterogeneous catalytic reaction. The adsorption energy was constant without any transmigration of the adsorbate

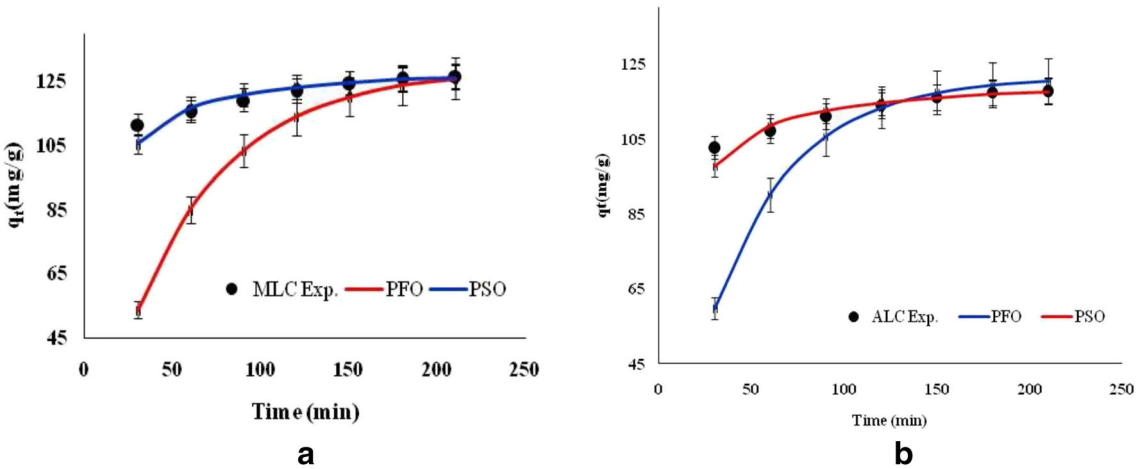

Fig. 4 Non-linear kinetic analysis of **a** MLC and **b** ALC biochar

Table 6 Isotherm parameters for Cr(VI) adsorption onto magnetic and activated biochar produced from *Lantana camara*

Isotherms	Parameters	MLC	ALC
A) Adsorption parameters			
Langmuir	q_m (mg/g)	102.03	94.69
	b (L/mg)	0.16	0.08
	R^2	0.991	0.994
	χ^2	0.005	0.001
	ARE	0.45	0.25
	RSME	0.05	0.04
Freundlich	K_f ($mg^{1-n}L^n/g$)	73.17	53.12
	$1/n$	0.63	0.62
	R^2	0.953	0.982
	$\chi 2$	0.015	0.002
	ARE	1.54	0.84
	RSME	0.08	0.13
Temkin	b (J/mol)	183.40	127.31
	K_T (L/g)	119.80	202.93
	R^2	0.952	0.979
	χ^2	0.034	0.041
	ARE	0.84	0.84
	RSME	1.85	1.42
B) Kinetics parameters			
Pseudo-first-order	$q_{e(cal)}$ (mg/g)	126.05	120.44
	K_{ad} (m^{-1})	0.37	0.33
	MPSD	0.06	0.04
	χ^2	10.98	4.91
	ARE	2.12	1.39
	RSME	8.08	17.66
Pseudo-second-order	$q_{e(cal)}$ (mg/g)	126.41	117.61
	K (g mg^{-1} min^{-1})	0.001	0.001
	MPSD	0.44	0.005
	χ^2	0.05	0.04
	ARE	0.27	0.19
	RSME	2.08	0.77

in the plane of the surface. The R_L (dimensionless constant) ranges from 0.003 to 0.0009 for MLC and 0.2–0.05 for ALC which indicates that Cr^{6+} uptake is favorable. The value R_L decreases with the increase in concentration which indicates that at high concentration the adsorption tends more towards irreversibility [33]. The higher value of Langmuir constant of MLC over ALC indicates the strong adsorption interaction between the adsorbent and adsorbate.

Separation factor or equilibrium parameter R_L can be denoted as

$$R_L = 1/(1 + bC_o) \quad (14)$$

where C_o= initial concentration; R_L value indicates adsorption nature (unfavorable if R_L>1, linear if R_L=1, favorable if 0<R_L<1, and irreversible if R_L=0). The R_L values for both the adsorbents are less than 1; hence, the adsorption is favorable. The Langmuir maximum adsorption capacity of MLC and ALC are 102.03 and 94.69 mg/g respectively.

3.6 Adsorption kinetics

Kinetic models have been used to investigate the mechanism of sorption and potential rate-controlling steps, which helps select an optimum contact time for the full-scale batch process. The behavior of adsorption kinetics of Cr^{6+} onto the surface of MLC and ALC biochars is depicted in Fig. 4a and b, respectively. Different kinetic reaction models, such as pseudo-first-order (PFO) and pseudo-second-reaction-order (PSO), are the most commonly used reaction models for sorption studies. The pseudo-first-order model assumes the rate of change of solute concentration with time (t) is directly proportional to the difference in saturation concentration and the amount of solid uptake with time. Pseudo-first-order rate equation and pseudo-second-order expression are expressed as Eqs. (15) and (16) Lagergren equation [57]:

$$q_e = q_e\left(1–\exp^{-K\mathrm{adt}}\right) \quad (15)$$

However, the pseudo-second-order equation can be given as:

$$t/q_e = (1/h) + t/q_e \quad (16)$$

where q_e = metal's mass adsorbed at equilibrium (mg/g), q_t= metal's mass at time t (min), K_{ad} is the rate constant of adsorption for first-order reaction (min^{-1}), h= Kqe^2, and K is the equilibrium rate constant of adsorption for pseudo-second-order (g mg^{-1} min^{-1}). The kinetic analysis has been performed using both model and the plot of q_e vs. t. Among both models, the results showed that pseudo-second-order kinetics fits best based on the error analysis such as root mean square error (RSME), Marquardt's percent standard deviation (MPSD), average relative error (ARE), and chi-square (χ^2) due to limitation overuse of R^2 value to solve non-linear plots. The lower the value for ARE and RSME, the better the data fits the isotherms. The calculated parameters of q_e, K_{ad}, and K obtained from both the models are summarized in Table 6. The results confirm that the rate of reaction is proportional to the number of adsorption sites on the adsorbent surface [14, 33]. The chemical adsorption of adsorbate on adsorbent may be the rate-limiting step in both ALC and MLC.

3.7 Adsorption mechanism

There are three possible mechanisms through which MLC works: (1) anion exchange; (2) reduction; and (3) electrostatic interaction. The presence of Cl within the biochar matrix due to the impregnation is exchanged with the Cr^{6+} [58]. Cr is also removed through a reduction mechanism where Cr^{6+} was reduced into Cr^{3+}. Due to the oxidation of Cr^{6+}, the ether and

carboxyl groups break down and produce hydroxyl groups on the MLC surface. When these negatively charged surfaces come in contact with the electron donor groups, Cr^{6+} is reduced to Cr^{3+}. Further oxidation of Fe^{2+} into Fe^{3+} ions promotes the conversion of Cr^{6+} into Cr^{3+} [40]. Substitution of Fe^{3+} with Cr^{3+}, complexation with surface functional groups, and formation of $Cr(OH)_3$ also play a vital role in adsorption. The absence of a new peak after Cr loading in XRD spectra suggests that no crystal was formed. Although electrostatic interaction is one of the prime adsorption mechanisms, some amount of Cr adsorption is caused by reduction and co-precipitation [10, 59]. From the adsorption study, it was revealed that modified biochar followed monolayer adsorption onto the surface of adsorbent via sharing or exchange of electrons. The presence of iron ions and functional groups on the surface of modified biochar is responsible for adsorption [41] and leads to Cr immobilization.

3.8 Desorption and reusability

To assess the commercial viability of the prepared biochar, it is important to evaluate the regeneration ability of the sorbent saturated with the concerned pollutant. The results indicated that desorption varied considerably among the adsorbents. It was observed that the removal efficiency of Cr^{6+} by ALC and MLC declined from 86.7 to 67.3% and from 83.6 to 57.8%, respectively, after the fourth cycle (Fig. 5). The decline in the removal efficiency after several cycles of adsorption-desorption might be due to formation of layers of hydroxide on the surface of adsorbent [60–62]. In alkaline solution, CrO_4^{2-} is the dominant form of Cr^{6+}, which can be exchanged by hydroxide (OH^-). Apart from this, electrostatic repulsion due to negatively charged adsorption sites increases desorption of Cr^{6+} from adsorbent. The desorption efficiency was higher in ALC (73.5%) than that in MLC (56%) which may be attributed to the strong affinity of Cr^{6+} ion for iron oxide on magnetic biochar [6]. Thus, it can be established that both MLC and ALC could be successfully reused.

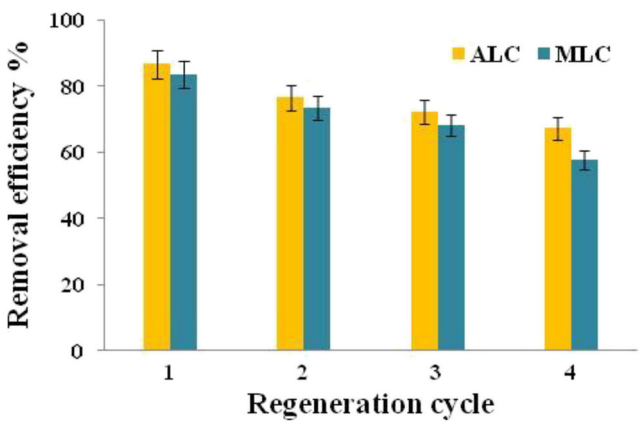

Fig. 5 Reusability capacity for ALC and MLC

Apart from all these, to fortify biochar's suitability as a sustainable adsorbent, techno-economic feasibility assessment and up-scaling its production from lab scale to commercial scale is essential. In the year 2019, the global biochar market was 1.39 billion USD which is expected to rise to 3.46 billion USD by 2025 [59]. The current growing interest for biochar as an adsorbent for wastewater treatment is expected to increase its demand thereby increasing its cost. From the study conducted by Krasucka et al. [60], it was observed that the cost of biochar production was 350–1200 USD/ton, which was lower than conventional activated carbon viz. 1100–1700 USD/ton [62]. According to studies, biochar production costs may range from 90 USD/ton to 8850 USD/ton [31]. Studies conducted on paper mill sludge [63], Willow [64], particleboard [34], Eggshell-modified biochar [10], etc. suggest that production of activated carbon from waste biomass is profitable compared to conventional activated carbon. Also, studies suggest that installation of production or treatment plant near to the point of source is more profitable compared to offsite [65, 66]. From an economic point of view, the market price of the biochar depends on several aspects such as the selected feedstock, pyrolysis production conditions, and transport, which considerably affect the production costs [67, 68]. Based on these studies, it can conclude that pyrolysis stage has a major share in the production cost (36%), followed by feedstock collection (12%) and transportation cost (9%). Thereby, the production cost can be reduced by the use of newer cheap production technologies coupled with the utilization of waste material as a cheap/low-cost feedstock [59]. Thus, weed-based biochar can be considered a feasible cheaper alternative to the more expensive activated carbons.

4 Conclusion

The current study deals with the conversion of *Lantana camara* biochar into low-cost adsorbent and its comparative evaluation for the adsorption phenomenon of magnetic biochar over activated biochar for the removal of chromium. The optimum values obtained from response surface methodology confirmed the higher chromium adsorption efficiency in magnetic biochar as compared to the activated biochar. The increase in adsorption efficiencies of metal ion chromium in magnetic biochar attributed to the impregnation of iron molecules on the biochar surfaces which enhanced the adsorption sites on its surfaces. Further, analysis of variance showed that reduction in removal efficiency (%) using both activated and magnetic biochar has an inverse relationship to the solution pH. The highest chromium removal was observed at pH 3.01. The optimum adsorption conditions obtained for maximum removal were as follows: pH = 3.01, an initial concentration of 161.23 mg/L, and a dose of 1.82 g/L. The maximum adsorption capacity of magnetic and activated biochar is 102.03

and 94.69 mg/g respectively. After adsorption, the exhausted/spent magnetic biochar composite could be easily collected by magnetic separation due to its excellent ferromagnetic properties.

Supplementary Information The online version contains supplementary material available at https://doi.org/10.1007/s13399-021-01448-3.

Acknowledgements The authors would like to acknowledge Tezpur University for providing the analytical facilities. The first author is also thankful to UGC, New Delhi, for providing the grant of the Rajiv Gandhi National Fellowship.

Declarations

Conflict of interest The authors declare no competing interests.

References

1. Bhuyan MS, Bakar MA, Islam MS, Akhtar A (2017) Heavy metal contamination in surface water and sediments of the Meghna River, Bangladesh. Environ Nanotechnol Monit Manag 8:273–279
2. US EPA (2009) National primary drinking water regulations. US Environmental Protection Agency, EPA 816-F-09–004
3. BIS report (2012) Drinking water-specification, Bureau of Indian Standards, IS-10500
4. Agrafioti E, Kalderis D, Diamadopoulos E (2014) Arsenic and chromium removal from water using biochars derived from rice husk, organic solid wastes and sewage sludge. J Environ Manag 133:309–314
5. Wang H, Wang S, Chen Z, Zhou X, Wang J, Chen Z (2020) Engineered biochar with anisotropic layered double hydroxide nanosheets to simultaneously and efficiently capture Pb^{2+} and CrO_4^{2-} from electroplating wastewater. Bioresour Technol 306: 123118
6. Dong X, Lena QM, Li Y (2011) Characteristics and mechanisms of hexavalent chromium removal by biochar from sugar beet tailing. J Hazard Mater 190:909–915
7. Ghorbani-Khosrowshahi S, Behnajady MA (2016) Chromium(VI) adsorption from aqueous solution by prepared biochar from *Onopordom Heteracanthom*. Int J Environ Sci Technol 13:1803–1814
8. Gupta S, Babu BV (2009) Removal of toxic metal Cr(VI) from aqueous solutions using sawdust as adsorbent: equilibrium, kinetics and regeneration studies. Chem Eng J 150:352–365
9. Dotto GL, Mckay G (2020) Current scenario and challenges in adsorption for water treatment. J Environ Chem Eng 8:103988
10. Çelebi H (2020) Recovery of detox tea wastes: usage as a lignocellulosic adsorbent in Cr^{6+} adsorption. J Environ Chem Eng 8: 104310
11. Celebi H, Gök O (2017) Use of aqis for adsorption of Pb from aqueous solution. Sigma 35:69–75
12. Çelebi H, Gök G, Gök O (2020) Adsorption capability of brewed tea waste in waters containing toxic lead (II), cadmium (II), nickel (II), and zinc (II) heavy metal ions. Sci Rep 10:1–12
13. Mohan D, Kumar H, Sarswat A, Alexandre-Franco M, Pittman CU (2014) Cadmium and lead remediation using magnetic oak wood and oak bark fast pyrolysis bio-chars. Chem Eng J 236:513–528
14. Ding Z, Hu X, Wan Y, Wang S, Gao B (2016) Removal of lead, copper, cadmium, zinc, and nickel from aqueous solutions by alkali-modified biochar: batch and column tests. J Ind Eng Chem 33:239–245
15. Tan G, Sun W, Xu Y, Wang H, Xu N (2016) Sorption of mercury (II) and atrazine by biochar, modified biochars and biochar based activated carbon in aqueous solution. Bioresour Technol 211:727–735
16. Trakal L, Veselskáa V, Šafarikb I, Vítkováa M, Cíhalováa S, Komárek M (2016) Lead and cadmium sorption mechanisms on magnetically modified biochars. Bioresour Technol 203:318–324
17. Ifthikar J, Wang J, Wang Q, Wang T, Wang H, Khan A, Jawad A, Sun T, Jiao X, Chen Z (2017) Highly efficient lead distribution by magnetic sewage sludge biochar: sorption mechanisms and bench applications. Bioresour Technol 238:399–406
18. Xiang W, Zhang X, Chen K, Fang J, He F, Hu X, Tsang DC, Ok YS, Gao B (2020) Enhanced adsorption performance and governing mechanisms of ball-milled biochar for the removal of volatile organic compounds (VOCs). Chem Eng J 385:123842
19. Zhang M, Gao B, Varnoosfaderani S, Hebard A, Yao Y, Inyang M (2013) Preparation and characterization of a novel magnetic biochar for arsenic removal. Bioresour Technol 130:457–462
20. Wang S, Gao B, Zimmerman A, Li Y, Ma L, Harris W, Migliaccio K (2015) Removal of arsenic by magnetic biochar prepared from pinewood and natural hematite. Bioresour Technol 175:391–395
21. Yaduraju NT, Sharma AR, Rao AN (2015) Weeds in Indian Agriculture: problems and prospects to become self sufficient. Indian Farming 65:02–06
22. Ghadge S, Jadhav B (2013) Effect of Lantana manures on nutrient content of fenugreek (*Trigonella foenum graecum* L.). Biosci Discov 4:189–193
23. Girish CR, Murty VR (2014) Adsorption of phenol from aqueous solution using *Lantana camara*, forest waste: kinetics, isotherm, and thermodynamic studies. Int Sch Res Notices 2014:1–16. https://doi.org/10.1155/2014/201626
24. Ravulapalli S, Kunta R (2018) Enhanced removal of chromium (VI) from wastewater using active carbon derived from *Lantana camara* plant as adsorbent. Water Sci Technol 78:1377–1389
25. Priyanka N, Joshi PK (2013) A review of *Lantana camara* studies in India. Int J Sci Res 3:1–11
26. Azargohar R, Dalai AK (2008) Steam and KOH activation of biochar: experimental and modeling studies. Microporous Mesoporous Mater 110:413–421
27. Januszewicz K, Kazimierski P, Klein M, Kardaś D, Łuczak J (2020) Activated carbon produced by pyrolysis of waste wood and straw for potential wastewater adsorption. Materials 13:2047
28. Baig SA, Zhu J, Muhammad N, Sheng T, Xu X (2014) Effect of synthesis methods on magnetic Kans grass biochar for enhanced As (III, V) adsorption from aqueous solutions. Biomass Bioenergy 71: 299–310
29. An Q, Li XQ, Nan HY, Yu Y, Jiang JN (2018) The potential adsorption mechanism of the biochars with different modification processes to Cr (VI). Environ Sci Pollut Res 25:31346–31357
30. Liou TH, Wang PY, Liou YH (2016) An effective method to enhance adsorption capacity and mesoporosity of activated carbon by pre-pyrolysis and chemical activation procedures. Bioresources 11: 6110–6124
31. Marchitan N, Cojocaru C, Mereuta A, Duca G, Cretescu I, Gonta M (2010) Modeling and optimization of tartaric acid reactive extraction from aqueous solutions: a comparison between response surface methodology and artificial neural network. Sep Purif Technol 75:273–285
32. Ahmed MB, Zhou JL, Ngo HH, Guo W (2016) Insight into biochar properties and its cost analysis. Biomass Bioenergy 84:76–86
33. Bordoloi N, Goswami R, Kumar M, Kataki R (2017) Biosorption of Co (II) from aqueous solution using algal biochar: kinetics and isotherm studies. Bioresour Technol 244:1465–1469

34. Park J, Hung I, Gan Z, Rojas OJ, Lim KH, Park S (2013) Activated carbon from biochar: Influence of its physicochemical properties on the sorption characteristics of phenanthrene. Bioresour Technol 149:383–389
35. Saha PD, Dey A, Marik P (2012) Batch removal of chromium (VI) from aqueous solutions using wheat shell as adsorbent: process optimization using response surface methodology. Desalin Water Treat 39:95–102
36. Dotto GL, Salau NPG, Piccin JS, Cadaval TRSA, de Pinto LAA (2017) Adsorption kinetics in liquid phase: modeling for discontinuous and continuous systems. In: Bonilla-Petriciolet A, Mendoza-Castillo DI, Reynel-Avila HE (eds) Adsorption Processes for Water Treatment and Purification. Springer, Chambridge, pp 53–76
37. Halim SFA, Kamaruddin AH, Fernando W (2009) Continuous biosynthesis of biodiesel from waste cooking palm oil in a packed bed reactor: optimization using response surface methodology (RSM) and mass transfer studies. Bioresour Technol 100:710–716
38. Montgomery DC (2017) Design and analysis of experiments, Fifth edn. Wiley, New York
39. Dotto GL, Cadaval TRS, Pinto LAA (2012) Preparation of bionanoparticles derived from Spirulina platensis and its application for Cr (VI) removal from aqueous solutions. J Ind Eng Chem 18:1925–1930
40. Hoang LP, Van HT, Nguyen LH, Mac DH, Vu TT, Ha LT, Nguyen XC (2019) Removal of Cr (VI) from aqueous solution using magnetic modified biochar derived from raw corncob. New J Chem 47: 18663–18672
41. Yang P, Guo D, Chen Z, Cui B, Xiao B, Liu S, Hu M (2016) Removal of Cr (VI) from aqueous solution using magnetic biochar synthesized by a single step method. J Dispers Sci Technol 38: 1665–1674
42. Zhang P, Zheng S, Liu J, Wang B, Liu F, Feng Y (2018) Surface properties of activated sludge-derived biochar determine the facilitating effects on Geobacter co-cultures. Water Res 142:441–451
43. Zhu W, Yu D, Shi M, Zhang Y, Huang T (2017) Quinone-mediated microbial goethite reduction and transformation of redox mediator, anthraquinone-2, 6-disulfonate (AQDS). Geomicrobiol J 34(1):27–36
44. Ifthikar J, Chen Z, Chen Z, Jawad A (2020) A self-gating proton-coupled electron transfer reduction of hexavalent chromium by core-shell SBA-Dithiocarbamate chitosan composite. J Hazard Mater 384:121257
45. Zhao N, Yin Z, Liu F, Zhang M, Lv Y, Hao Z, Pan G, Zhang J (2018) Environmentally persistent free radicals mediated removal of Cr (VI) from highly saline water by corn straw biochars. Bioresour Technol 260:294–301
46. Ifthikar J, Shahib II, Sellaoui L, Jawad A, Zhao M, Chen Z, Chen Z (2020) pH tunable anionic and cationic heavy metal reduction coupled adsorption by thiol cross-linked composite: physicochemical interpretations and fixed-bed column mathematical model study. Chem Eng J 401:126041
47. Zheng C, Yang Z, Si M, Zhu F, Yang W, Zhao F, Shi Y (2021) Application of biochars in the remediation of chromium contamination: fabrication, mechanisms, and interfering species. J Hazard Mater 407:124376
48. Sharma DC, Forster CF (1994) The treatment of chromium wastewaters using the sorptive potential of leaf mould. Bioresour Technol 49:31–40
49. Barrera-Díaz CE, Lugo-Lugo V, Bilyeu B (2012) A review of chemical, electrochemical and biological methods for aqueous Cr (VI) reduction. J Hazard Mater 223:1–12
50. Regmi P, Moscoso JLG, Kumar S, Cao X, Mao J, Schafran G (2012) Removal of copper and cadmium from aqueous solution using switchgrass biochar produced via hydrothermal carbonization process. J Environ Manag 109:61–69
51. Namasivayam C, Prabha D, Kumutha M (1998) Removal of direct red and acid brilliant blue by adsorption on to banana pith. Bioresour Technol 64:77–79
52. Frolova L, Kharytonov M (2019) Synthesis of magnetic biochar for efficient removal of Cr(III) cations from the aqueous medium. Adv Mater Sci Eng:1687–8434. https://doi.org/10.1155/2019/2187132
53. Lim SF, Zheng YM, Chen JP (2009) Organic arsenic adsorption onto a magnetic sorbent. Langmuir 25:4973–4978
54. Segal LGJMA, Creely JJ, Martin AE Jr, Conrad CM (1959) An empirical method for estimating the degree of crystallinity of native cellulose using the X-ray diffractometer Text. Res J 29:786–794
55. Machala L, Tucek J, Zboril R (2011) Polymorphous transformations of nanometriciron(III) oxide: a review. Chem Mater 23:3255–3272
56. Dada AO, Olalekan AP, Olatunya AM, Dada O (2012) Langmuir, Freundlich, Temkin and Dubinin–Radushkevichn isotherms studies of equilibrium sorption of Zn^{2+} unto phosphoric acid modified rice husk. IOSR J Appl Chem 3(1):38–45
57. Ho YS, Ofomaja AE (2006) Pseudo-second-order model for lead ion sorption from aqueous solutions onto palm kernel fiber. J Hazard Mater 129:137–142
58. Khitous M, Salem Z, Halliche D (2016) Effect of interlayer anions on chromium removal using Mg–Al layered double hydroxides: kinetic, equilibrium and thermodynamic studies. Chin J Chem Eng 24:433–445
59. He R, Yuan X, Huang Z, Wang H, Jiang L, Huang J, Tan M, Li H (2019) Activated biochar with iron-loading and its application in removing Cr (VI) from aqueous solution. Colloids Surf A Physicochem Eng Asp 579:123642
60. Daneshvar E, Zarrinmehr MJ, Kousha M, Hashtjin AM, Saratale GD, Maiti A, Vithanage M, Bhatnagar A (2019) Hexavalent chromium removal from water by microalgal-based materials: adsorption, desorption and recovery studies. Bioresour Technol 293: 122064
61. Akram M, Bhatti HN, Iqbal M, Noreen S, Sadaf S (2017) Biocomposite efficiency for Cr (VI) adsorption: kinetic, equilibrium and thermodynamics studies. J Environ Chem Eng 5:400–411
62. Nakagawa T, Kokubo K, Moriwaki H (2014) Application of fullerenes-extracted soot modified with ethylenediamine as a novel adsorbent of hexavalent chromium in water. J Environ Chem Eng 2:1191–1198
63. Fdez-Sanromán A, Pazos M, Rosales E, Sanromán MA (2020) Unravelling the environmental application of biochar as low-cost biosorbent: a review. Appl Sci 10:7810
64. Krasucka P, Pan B, Ok YS, Mohan D, Sarkar B, Oleszczuk P (2021) Engineered biochar-a sustainable solution for the removal of antibiotics from water. Chem Eng J 405:126926
65. Thompson KA, Shimabuku KK, Kearns JP, Knappe DRU, Summers RS, Cook SM (2016) Environmental comparison of biochar and activated carbon for tertiary wastewater treatment. Environ Sci Technol 50:1253–11262
66. Manyuchi MM, Chaukura N, Ruzvidzo C (2016) Techno-economic assessment for biochar production from paper mill sludge. Research Intellectual Outputs 2016-Science. Engineering and Technology 5, National University of Science and Technology, NUST Bulawayo
67. Kuppens T, Van Dael M, Vanreppelen K, Thewys T, Yperman J, Carleer R, Van Passel S (2015) Techno-economic assessment of fast pyrolysis for the valorization of short rotation coppice cultivated for phytoextraction. J Clean Prod 88:336–344
68. Keske C, Godfrey T, Hoag DL, Abedin J (2020) Economic feasibility of biochar and agriculture coproduction from Canadian black spruce forest. Food Energy Secur 9(1):e188